Thin Solid Films 807 (2024) 140554

Contents lists available at ScienceDirect

Thin Solid Films

journal homepage: www.elsevier.com/locate/tsf

Growth and characterization of $Sb_2(S_xSe_{1-x})_3$ thin films prepared by chemical-molecular beam deposition for solar cell applications

T.M. Razykov [a], K.M. Kuchkarov [a], B.A. Ergashev [a], Lukas Schmidt-Mende [b], Tim Mayer [b], M. Tivanov [c], M. Makhmudov [a], D.Z. Isakov [a], R. Khurramov [a], M. Primmatov [a], K.F. Shakhriev [a], Sh.B. Utamuradova [d], R.T. Yuldoshov [a,*]

[a] Physical-Technical Institute, Chingiz Aytmatov Street 2B, Tashkent 100084, Uzbekistan
[b] University of Konstanz, Universitäts str 10, Faculty of Physics Fach, 680D-78457 Konstanz, Germany
[c] Faculty of Physics, Belarusian State University, 220030 Minsk, Belarus
[d] Institute of Semiconductors Physics and Microelectronics, Yangi Olmazor Street 20, Tashkent 100057, Uzbekistan

ARTICLE INFO

Keywords:
Antimony sulfide selenide
Chemical molecular beam deposition
Band gap
Absorbance
Photovoltaics

ABSTRACT

Antimony sulfide selenide, $Sb_2(S_xSe_{1-x})_3$ ($x = 0$–1), is a tunable bandgap compound that combines the advantages of antimony sulfide (Sb_2S_3) and antimony selenide (Sb_2Se_3). This material shows great potential as a light-absorbing material for low-cost, low-toxicity, and highly stable thin-film solar cells. In this study, $Sb_2(S_xSe_{1-x})_3$ thin films were deposited by chemical-molecular beam deposition on soda-lime glass substrates using antimony (Sb), selenium (Se), and sulfur (S) precursors at a substrate temperature of 420 °C. By independently controlling the source temperatures of Sb, Se, and S, $Sb_2(S_xSe_{1-x})_3$ thin films with varying component ratios were obtained. Scanning electron microscopy revealed significant changes in the surface morphology of the films depending on the elemental ratio of [S]/([S]+[Se]). Crystallites shaped like cylindrical microrods with $d = 0.5$–2 μm diameter and $l = 3$–5 μm length were grown at a certain angle on the substrate. X-ray diffraction patterns showed peaks corresponding to the orthorhombic structures of Sb_2Se_3, Sb_2S_3 and their ternary compounds $Sb_2(S_xSe_{1-x})_3$. The optical characterization revealed a high absorption coefficient of 10^5 cm^{-1} in the visible and near-infrared light regions. The band gap of the compounds changed almost linearly from 1.2 eV to 1.36 eV with a change in the ratio of elements [S]/([S]+[Se]) from 0.03 to 0.08.

1. Introduction

Currently, researchers are paying special attention to the use of chalcogenide binary compounds antimony selenide (Sb_2Se_3), antimony sulfide (Sb_2S_3), and antimony sulfide-selenide ($Sb_2(S_xSe_{1-x})_3$) as an absorbing layer for solar cells. This is due to the fact that the physical properties (p-type conductivity, band gap E_g=1.1–1.8 eV, a high absorption coefficient α>10^5 cm^{-1} (in the visible and near-infrared region of solar radiation), low melting point (Sb_2Se_3 – 612 °C, Sb_2S_3 – 550 °C) are very close to the properties of widely used material $Cu(In,Ga)(Se,S)_2$ in the solar cells field [1,2]. In addition, these materials have relatively inexpensive elements (abundant in nature), are stable under external influences, and non-toxic [3,4], which opens up the possibility of using them to produce solar cells on an industrial scale that are both highly efficient and environmentally friendly. In recent years, the introduction of innovative structures and methods for producing $Sb_2(S_xSe_{1-x})_3$ thin films has led to an increase in the efficiency of solar cells.

$Sb_2(S_xSe_{1-x})_3$ thin films have been prepared by various methods: thermal evaporation [5,6], co-evaporation [7], rapid thermal evaporation [8,9], close space sublimation [10,11], pulsed laser deposition [12], vapor transport deposition [13-15] and chemical methods. However, changing the composition ratio of films produced by these methods and achieving the required high vacuum conditions can be challenging, leading to intricate procedures.

Therefore, non-vacuum approaches have also been explored for the deposition of $Sb_2(S_xSe_{1-x})_3$ thin films. Techniques such as chemical beam deposition (CBD), spin-coating of sol–gel precursors, and other solution-based methods have been utilized. For instance, the injection chemical bath deposition (ICBD) method has been developed based on the CBD method [16]. By optimizing the injection time and the amount of Se

* Corresponding author.
E-mail address: yuldoshovruhiddin@gmail.com (R.T. Yuldoshov).

https://doi.org/10.1016/j.tsf.2024.140554
Received 16 April 2024; Received in revised form 24 September 2024; Accepted 12 October 2024
Available online 13 October 2024

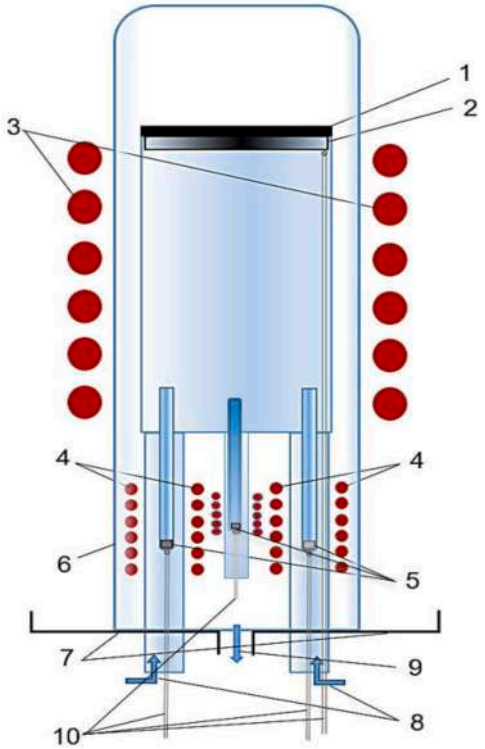

Fig. 1. Schematic representation of the reactor device for producing antimony chalcogenide thin films.
1, 2 – substrate and holder, 3 – substrate heater, 4 – source heaters, 5 – sources of evaporated components, 6 – reactor cap, 7 – flange, 8 – hydrogen gas inlet (H_2), 9 – hydrogen gas outlet, 10 – thermocouples respectively.

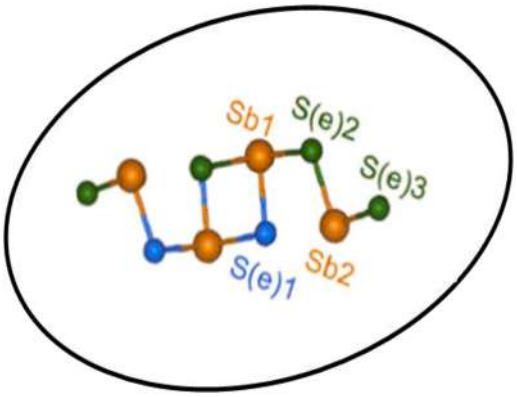

Fig. 2. The crystal structure of $Sb_2(S_xSe_{1-x})_3$ non-equivalent atomic sites in each $[Sb_4{\times}_6]_n$ ($X = S$, Se) atomic chain. [22].

source, $Sb_2(S_xSe_{1-x})_3$ thin films with a V-shaped gradient band gap structure were fabricated. This structure enhances carrier transport and light capture within the films, boosting open circuit voltage, short-circuit current density, and fill factor. An ICBD-$Sb_2(S_xSe_{1-x})_3$ device with a full-inorganic architecture of FTO/CdS/$Sb_2(S,Se)_3$/PbS/-Carbon was fabricated, achieving a maximum efficiency of 7.63 %. To further improve the crystallinity of these thin films, various annealing methods are employed following the initial deposition. Annealing is a crucial step in thin film processing as it helps to enhance crystal growth, reduce defects, and improve the overall structural and electronic properties of the films. Traditional selenium vapor-assisted annealing has been commonly used, but it presents limitations in heat conduction and selenium activity.

Recent advancements have introduced liquid medium annealing [17], which demonstrates superior heat conduction and higher selenium activity compared to traditional vapor-assisted annealing. Liquid medium annealing induces a highly preferred [041]/[141] orientation in Sb_2S_3, significantly enhancing carrier transport efficiency and reducing potential shunt paths, thus improving the overall performance of the films.

In this study, non-vacuum chemical molecular beam deposition (CMBD) method is used to produce ternary compounds $Sb_2(S_xSe_{1-x})_3$ films for solar cell applications. This method enables the production of thin films with different compositions by adjusting parameters such as synthesis time, substrate and source temperatures, and carrier gas flow rate. Moreover, the efficiency of solar cells is linked to the structural, morphological, and optical properties of the absorber thin film. Ultimately, $Sb_2(S_xSe_{1-x})_3$ thin films are utilized with an appropriate [S]/([S]+[Se]) ratio as the efficient light absorber material for solar cells due to their tunable bandgap from 1.2 to 1.35 eV, p-type conductivity, high absorption coefficient. It is anticipated that the outcomes of this study will contribute to the advancement of this promising semiconductor material. Recently, we have discussed fabrication of Sb_xSe_y films by CMBD and their characteristics [18,19]. In this work, we investigated the influence of the [S]/([S]+[Se]) ratio on the structural, morphological, and optical properties of samples. The composition of the film is varied by adjusting selenium and sulfur source temperatures in hydrogen flow at atmospheric pressure.

2. Experiment

$Sb_2(S_xSe_{1-x})_3$ films are obtained by the CMBD method from separate sources of the elements antimony (Sb), sulfur (S), and selenium (Se) (99.999 % purity, Chemsavers) at a substrate temperature of 420 °C in a hydrogen environment [20,21]. Soda-lime glass (SLG) substrates were cleaned using acetone (99.5 % purity), ethanol (99.9 % purity) and deionized water in an ultrasonic bath, then dried with N_2 gas. The Sb, S, and Se precursors were loaded into the growth chamber. The system is then brought into working condition and purged with hydrogen due to its high thermal conductivity, lightness, and small molecular diameter, which helps remove atmospheric and polluting gases. Because of these properties, the growth rate of the $Sb_2(S_xSe_{1-x})_3$ layer in an H_2 environment is 2–3 times higher than in other inert gases such as Ar or He. Hydrogen gas flow rate of 20 cm^3/min was controlled by Gas Flow Measurement "Zach Metalchem". Initially, $Sb_2(S_xSe_{1-x})_3$ thin films were deposited at different source temperatures of sulfur and selenium. This data provides temperature information for different sources of sulfur and selenium at various ratios. Specifically, for the deposition of x = 0.03, 0.04, 0.08 samples, the temperature of the sulfur source was 310 °C, 320 °C, and 370 °C, while the temperature of the selenium source was 455 °C, 440 °C, and 425 °C, respectively. Once the substrate reached the required temperature, the individual heater for the evaporator was turned on to regulate its temperature. The deposition process was conducted for 30 min. All these temperature ratios are in relation to the source temperature of antimony, which is consistently stated as 850 °C. At the Sb (850 °C) and Se (425–455 °C) and S (310–370 °C) evaporation temperatures, granules transform into the vapour phase:

$$Sb(s) + 2Se(s) + 2S(s) + H_2 = Sb(g) + Se_2(g) + S_2(g) + H_2 \quad (1)$$

$Se_2(g)$ and $S_2(g)$ reacts with hydrogen, and hydrogen selenide and hydrogen sulfide are formed:

$$Se_2(g) + S_2(g) + 4H_2 = 2H_2Se(g) + 2H_2S(g) \quad (2)$$

Sb and Se and S atoms and H_2Se and H_2S molecules cover the surface of the substrate, and $Sb_2(S_xSe_{1-x})_3$ films are formed as a consequence of their interaction:

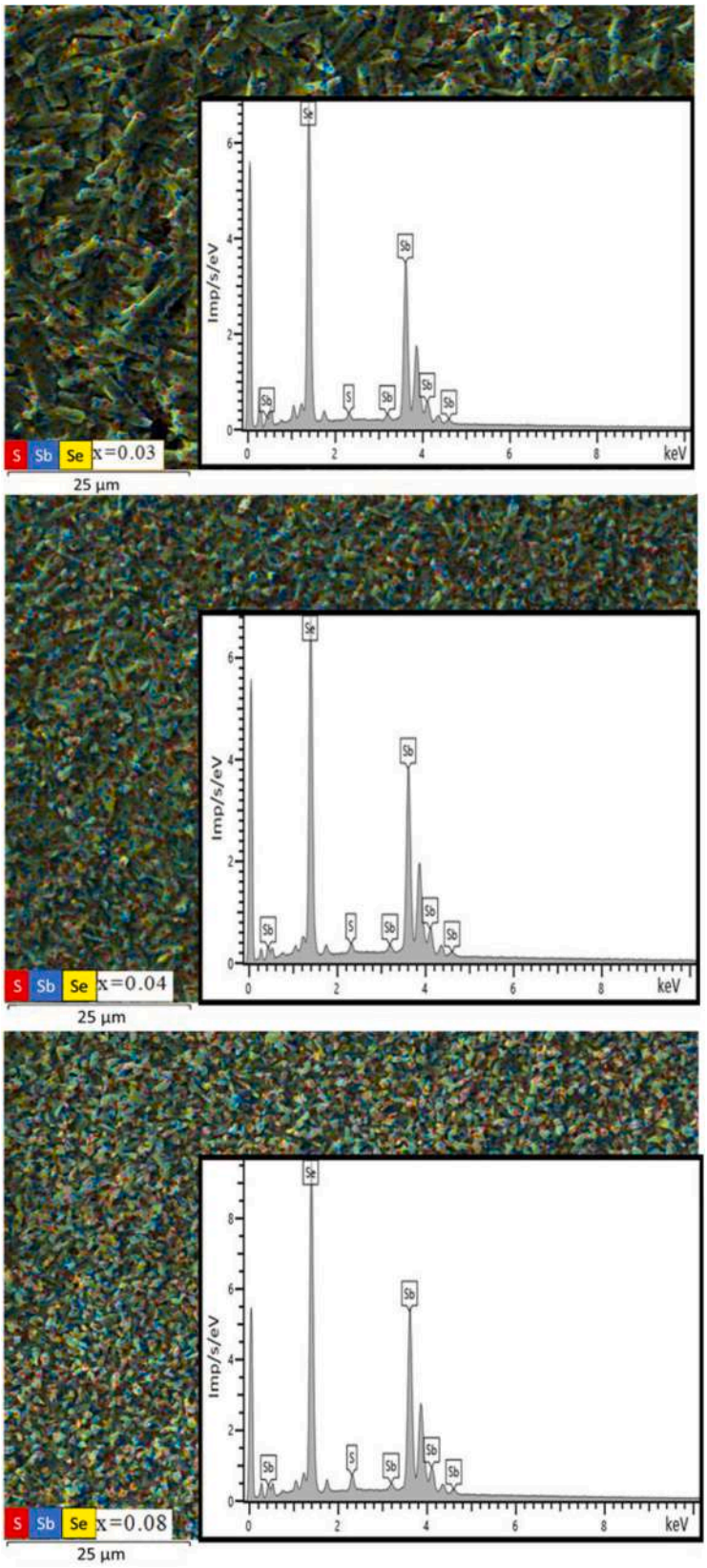

Fig. 3. Typical EDX spectra of synthesized $Sb_2(S_xSe_{1-x})_3$ thin films.

$$2Sb(g) + (1\text{-}x)Se_2(g) + xS_2(g) + H_2Se(g) + H_2S(g) = Sb_2(S_xSe_{1-x})_3\,(s) + 2H_2 \quad (3)$$

The composition of S and Se on $Sb_2(S_xSe_{1-x})_3$ films was controlled by changing the S/ (*S*+Se) ratios in the vapour phase mixture of Sb and Se and S (evaporated amount), which was varied by the molecular beam flux of Se and S.

Fig. 1 shows schematic representation of the device to produce antimony chalcogenide thin films. Using the CMBD method as a base, it

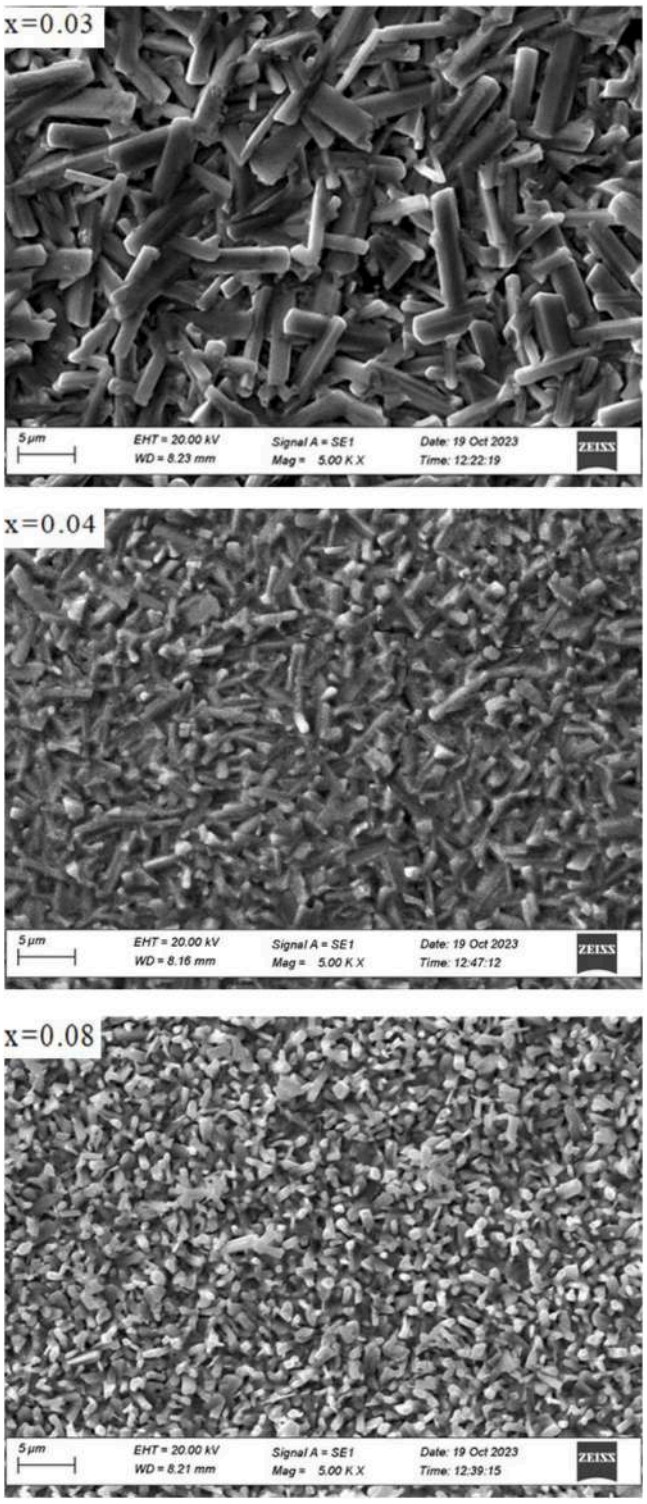

Fig. 4. Morphology of $Sb_2(S_xSe_{1-x})_3$ thin films.

is possible to create a thin film with a surface area of 50 cm^2. The size of the surface area can be further increased by making additional adjustments to the quartz tube and in quartz reaction chamber.

The surface morphology of the $Sb_2(S_xSe_{1-x})_3$ films was examined by using LEO-1455 VP (Carl Zeiss) model scanning electron microscope (SEM) instrument in secondary electrons mode, operating voltage used for imaging is 20 kV. The elemental composition of synthesized $Sb_2(S_xSe_{1-x})_3$ films was determined using Energy Dispersive X-ray (EDX) spectroscopy analysis with an Aztec Energy Advanced Spectrometer having energy spectral resolution of 127 eV and chemical element determining sensitivity of 0.5 wt.%. Phase identification was carried out by comparing the experimentally determined interplanar distances with tabular values from the database of the Joint Committee for the Powder Diffraction Standard (JCPDS). The X-ray diffraction (XRD) patterns were obtained from Rigaku Ultima IV X-ray diffractometer in the grazing incidence diffraction geometry at 1° of incident X-rays using CuK_α radiation ($\lambda = 0.15418$ nm) in the 2θ range of 10–60° with a step of 0.05°. The Raman spectra were measured by spectrometer Nanofinder HE (LOTIS TII) with 532 nm solid-state laser for excitation. The optical absorption spectra of the samples are taken at room temperature with the help of UV–Vis–NIR spectrophotometer Shimadzu UV-1900i.

3. Results and discussions

The crystal structure of $Sb_2(S_xSe_{1-x})_3$ is characterized by a Quasi-One-Dimensional configuration, where infinite chains of atoms stack together. This structure has low symmetry and is described by two distinct Sb sites and three S (Se) sites for each atomic unit [22,23,24]. In the mixed-anion $Sb_2(S_xSe_{1-x})_3$ component, S and Se atoms share the same positions, so the anion sites, denoted as site 1, site 2, and site 3, can be occupied by either S or Se atoms in Special Quasi-random Structures (Fig. 2). In addition to the arrangement of atoms within the crystal structure, it is mentioned that the atomic chains in $Sb_2(S_xSe_{1-x})_3$ interact with each other through van der Waals forces. Van der Waals forces are weak intermolecular forces that arise due to fluctuations in electron distributions. They are responsible for various phenomena, including the interaction between atoms or molecules nearby. In the case of $Sb_2(S_xSe_{1-x})_3$, the Van der Waals forces play a role in the interaction between the atomic chains, contributing to the stability and overall behavior of the crystal structure. These forces are relatively weak compared to other chemical bonds, such as covalent or ionic bonds, but they can still have a significant impact on the properties of materials, including their mechanical, thermal, and electrical characteristics.

To determine the precise compositions of the thin films, EDX spectroscopy was utilized. The spectra obtained from multiple areas of the films exhibited characteristic peaks corresponding to Sb, S, Se elements. The peak intensities were quantitatively analyzed to determine the relative concentrations of each element. The results demonstrated that the $Sb_2(S_xSe_{1-x})_3$ films consisted of a binary mixture of sulfur and selenium, with antimony as the main component. The relative concentrations of sulfur and selenium were found to vary within the film, indicating spatial variations in the composition. This information is crucial for understanding the stoichiometry of the films and its impact on the materials properties.

In Fig. 3 are presented the EDX results of $Sb_2(S_xSe_{1-x})_3$ thin films with S/(Se+*S*) ratios of $x = 0.03$, 0.04 and 0.08 respectively. The $Sb_2(S_xSe_{1-x})_3$ thin films synthesized at a high substrate temperature, involve challenges in maintaining their original stoichiometry due to the disparate vapor pressures of Sb, S, and Se. Notably, the higher vapor pressure of S in the high-temperature range results in S preferentially escaping during deposition, leading to S deficiency in the films.

Fig. 3 illustrates that the quantity of Sb in the thin films remains consistent across all samples. Consequently, we attribute significance to the alteration of the S/(Se+*S*) ratio within the thin film compositions and proceeded to calculate its variations.

Fig. 4 shows SEM images of thin films of $Sb_2(S_xSe_{1-x})_3$ grown at different ratio of the elements. Microcrystals on the surface of the films are evenly distributed over the substrate and the surface of the films becomes smoother and more compact with individual evaporation of the elements.

The morphology of the film surface also changes depending on the element ratio [S]/([S]+[Se]). Particles constituting the film have the shape of micro-rods with a diameter from 0.5 to 2 μm and a length from 3 to 5 μm with a certain angle relative to the substrate. When changing the ratio of components [S]/([S]+[Se])=0.04 on the surface of the films,

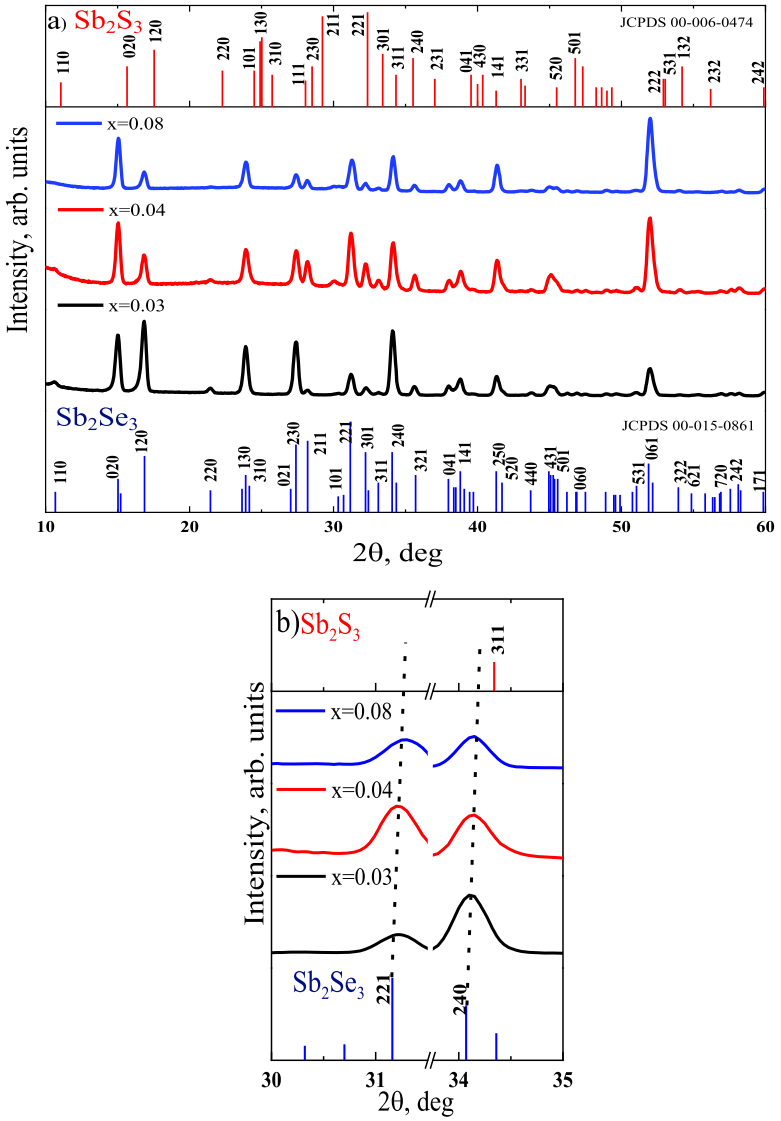

Fig. 5. a) XRD patterns of the $Sb_2(S_xSe_{1-x})_3$ thin films; b) enlarged (221) and (240) peaks of the same films as in panel a).

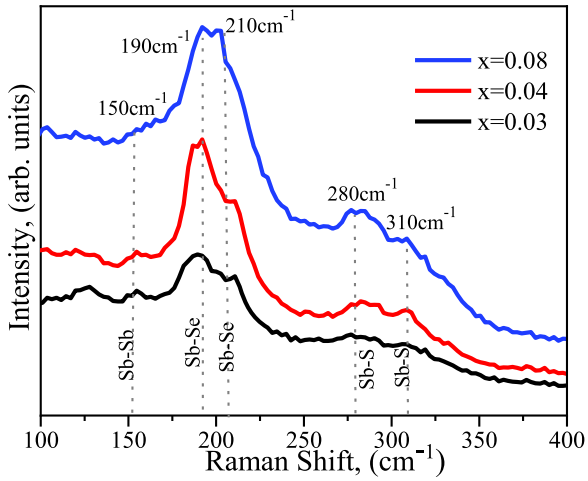

Fig. 6. Raman scattering spectra of $Sb_2(S_xSe_{1-x})_3$ samples.

the absence of inter crystalline voids and high compactness of crystallites is revealed and cylindrical microrods were epitaxial synthesized on the substrate with a near-perpendicular orientation.

Crystallites have a different growth orientation and show decreased rods lengths of 1 to 3 μm and a diameter of 0.5 to 1 μm. The ratio of a composition starting at 0.08, the introduction of a higher quantity of S in the $Sb_2(S_xSe_{1-x})_3$ film composition resulted in a reduction in grain size and characterized dense, more columnar structure. This can be attributed to the growth of crystallites with their c-axis in a direction perpendicular to the substrate.

Fig. 5 shows X-ray diffraction patterns of $Sb_2(S_xSe_{1-x})_3$ films obtained under various ratio of components [S]/([S]+[Se]). All detected peaks in the X-ray diffraction patterns correspond to the compounds Sb_2Se_3 and Sb_2S_3, as well as their ternary compounds $Sb_2(S_xSe_{1-x})_3$. It has been established that all $Sb_2(S_xSe_{1-x})_3$ have an orthorhombic structure with space group *Pnma*. In general, the study shows that the morphology and structure of $Sb_2(S_xSe_{1-x})_3$ thin films significantly depend on the synthesis conditions and ratio of the components.

Alteration of the temperature source for S from 310 °C to 370 °C induces a shift in the molar composition of S atoms within $Sb_2(S_xSe_{1-x})_3$, as evident from the X-ray diffraction patterns illustrated in Fig. 5. This, in turn, influences the variation in lattice parameters. Additionally, a discernible shift in the peaks is observed within the X-ray diffraction

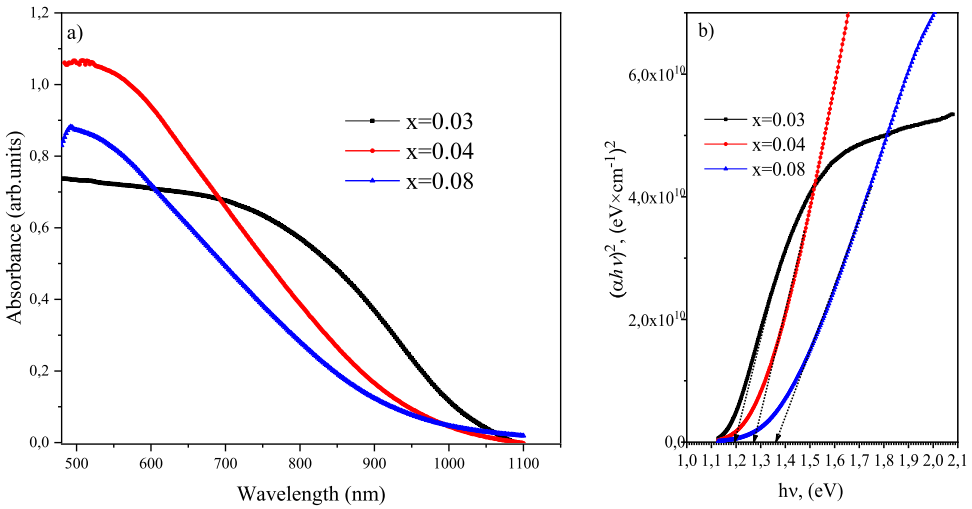

Fig. 7. a) Absorbance for $Sb_2(S_xSe_{1-x})_3$ thin films; b) Tauc plots of $Sb_2(S_xSe_{1-x})_3$ thin films.

pattern. Specifically, the peak shift is observed to move towards an increased maximum value of 2θ angle, which can be attributed to a reduction in the interplanar distance of crystallite and, correspondingly, a modification in the lattice parameters (Fig. 5b). This shift is primarily caused by the replacement of larger Se atoms with smaller S atoms, leading to a decrease in the lattice constants [24]. Moreover, an escalation in the [S]/([S]+[Se]) ratio intensifies the magnitude of the peaks labeled as (211) and (221). As visible from the figure, the X-ray diffraction patterns show the main strong peaks (221), (211); and secondary weak peaks (110), (020), (220), (240), and (621), which change noticeably with changing [S]/([S]+[Se]) ratio. In addition, all films showed a preferred (221) orientation, which was demonstrated to be beneficial for charge carrier transport. As the [S]/([S]+[Se]) ratio increased from 0.03 to 0.08, the decrease in the intensity of the (hk0) peaks ((230), (240)) was observed. This can be attributed to the growth of crystals in a direction perpendicular to the substrate.

Fig. 6 shows the combined scattering spectrum of $Sb_2(S_xSe_{1-x})_3$ thin films with different component ratios [S]/([S]+[Se]). Raman spectroscopy reveals intensity peaks at 150 cm^{-1}, 190 cm^{-1}, 210 cm^{-1}, 280 cm^{-1} and 310 cm^{-1} in all thin films of $Sb_2(S_xSe_{1-x})_3$. The basic lattice structure retained in the grown samples, and the results obtained for $Sb_2(S_xSe_{1-x})_3$ thin films showed good agreement with previous studies.

It was previously reported that the peaks at 190 cm^{-1} and 210 cm^{-1}, observed in the spectrum, are related to the vibrational modes of Sb-Se [25]. A peak with a frequency of 150 cm^{-1} indicates the presence of Sb-Sb vibrational modes in thin layers [26]. It was also found that the peaks at 280 cm^{-1} and 310 cm^{-1} correspond to the Sb-S vibrational modes [27]. With increasing values of the [S]/([S]+[Se]) ratio in thin films, a rise in the intensity of the peaks at 280 cm^{-1} and 310 cm^{-1} is observed. Fig. 7a) shows the optical absorbance spectra of $Sb_2(S_xSe_{1-x})_3$ films deposited at different ratio. The investigation focuses on the absorption spectrum recorded within the wavelength range of 450 nm to 1100 nm, utilizing a step size of 1 nm.

By utilizing the obtained absorbance data, the absorption coefficient (α) of the thin films was determined. It was assumed that the films exhibited a direct allowed band-to-band transition. To gain insights into the behavior of the films, the relationship between the functions $(\alpha h\nu)^n$ and f(hν) was established and graphically represented in Fig. 7b). The analysis of figure reveals a distinct absorption edge, indicating that the band gap arises primarily from the intrinsic transition within the $Sb_2(S_xSe_{1-x})_3$ films, rather than being influenced by extraneous impurities. To estimate the band gap energy (E_g) of the layers, the Tauc formula was used, expressed as follows:

$$(\alpha h\nu)^2 = A(h\nu - E_g) \quad (4)$$

Here, $h\nu$ denotes the energy of the incident photon, while A represents a constant, α – absorption coefficient. By extrapolating the linear regions of these graphs to the energy axis, one can determine the band gap energy.

The determined E_g values of $Sb_2(S_xSe_{1-x})_3$ films were increased from 1.2 to 1.36 eV According to Shockley–Queisser limit, photovoltaic performance of solar cells reaches a maximum, when the band gap of absorber layer is 1.34–1.4 eV [28]. It is evident that the variation in the band gap energy within the films is associated with changes in the [S]/([S]+[Se]) elemental ratio. These findings demonstrate the influence of the [S]/([S]+[Se]) ratio on the band gap energy of the $Sb_2(S_xSe_{1-x})_3$ films. The results contribute to a deeper understanding of the optical properties of these films and provide valuable insights for potential applications in optoelectronic devices.

4. Conclusion

The work explored the deposition of $Sb_2(S_xSe_{1-x})_3$ thin films using the non-vacuum CMBD method, introducing a versatile approach for tuning their composition. The morphology and structure of the films depend significantly on synthesis conditions and the [S]/([S]+[Se]) elemental ratio observed. The X-ray diffraction patterns confirmed the orthorhombic structure of $Sb_2(S_xSe_{1-x})_3$, showing promising preferred orientations for charge carrier transport. Raman spectroscopy revealed vibrational modes corresponding to Sb-Se and Sb-S bonds. Notably, varying the [S]/([S]+[Se]) ratio influenced the band gap energy, providing a tunable parameter for optoelectronic applications. The band gap (E_g) for $Sb_2(S_xSe_{1-x})_3$ thin films that we obtain were from 1.2 to 1.36 eV by changing the ratio of [S]/([S]+[Se]).

CRediT authorship contribution statement

T.M. Razykov: Writing – review & editing, Writing – original draft, Supervision, Project administration, Methodology, Conceptualization. **K.M. Kuchkarov:** Resources, Methodology, Investigation, Funding acquisition, Conceptualization. **B.A. Ergashev:** Methodology. **Lukas Schmidt-Mende:** Writing – review & editing, Supervision, Data curation. **Tim Mayer:** Writing – review & editing. **M. Tivanov:** Writing – original draft, Data curation. **M. Makhmudov:** Investigation. **D.Z. Isakov:** Investigation. **R. Khurramov:** Writing – review & editing, Writing – original draft, Investigation, Funding acquisition. **M. Primmatov:** Investigation. **K.F. Shakhriev:** Formal analysis. **Sh.B. Utamuradova:** Funding acquisition. **R.T. Yuldoshov:** Writing – original draft, Resources, Investigation, Funding acquisition, Formal analysis, Conceptualization.

Declaration of competing interest

The authors declare the following financial interests/personal relationships which may be considered as potential competing interests:

R.T. Yuldoshov reports financial support was provided by the Basic Research Program of the Academy of Sciences of the Republic of Uzbekistan, Ministry of innovative development of the Republic of Uzbekistan (Grant N№ FZ-2,020,102,944) and the State Research Program of the Republic of Belarus "Material Science, New Materials and Technologies".

Acknowledgements

This work was supported by the Basic Research Program of the Academy of Sciences of the Republic of Uzbekistan, Ministry of innovative development of the Republic of Uzbekistan (Grant N№ FZ-2020102944) and the State Research Program of the Republic of Belarus "Material Science, New Materials and Technologies".

Data availability

The data that has been used is confidential.

References

[1] Xiaomin Wang, Rongfeng Tang, Chunyan Wu, Development of antimony sulfide–selenide $Sb_2(S,Se)_3$ -based solar cells, J. Energy Chem. 27 (2018) 713–721.
[2] Alessio Bosio, Gianluca Foti, Stefano Pasini, Donato Spoltore, A review on the fundamental properties of Sb_2Se_3-based thin film solar cells, Energies. (Basel) 16 (2023) 6862.
[3] Abdurashid Mavlonov, Takhir Razykov, Fazal Raziq, A review of Sb_2Se3 photovoltaic absorber materials and thin-film solar cells, Solar Energy 201 (2020) 227–246.
[4] M.S. Tivanov, T.M. Razykov, K.M. Kuchkarov, D.S. Bayko, I.A. Kaputskaya, R. T. Yuldoshov, M.P. Pirimmetov, Effect of the Sb/Se ratio on the structural and electrical properties of Sb_xSe_y films, Appl. solar energy 59 (2023) 595–603.
[5] E.A. El-Sayad, Compositional dependence of the optical properties of amorphous $Sb_2Se_{3-x}S_x$ thin films, J. Non. Cryst. Solids. 354 (2008) 3806–3811, https://doi.org/10.1016/j.jnoncrysol.2008.05.004.
[6] K. Yang, B. Li, G. Zeng, Effects of substrate temperature and SnO_2 high resistive layer on Sb_2Se_3 thin film solar cells prepared by pulsed laser deposition, Solar Energy Materials and Solar Cells (2020) 110381, https://doi.org/10.1016/j.solmat.2019.110381.
[7] Y. Yin, C. Jiang, Y. Ma, R. Tang, X. Wang, L. Zhang, Z. Li, C. Zhu, T. Chen, Sequential co-evaporation and deposition of antimony selenosulfide thin film for efficient solar cells, Adv. Materials 202006689 (2021), https://doi.org/10.1002/adma.202006689.
[8] M. Ishaq, H. Deng, S. Yuan, H. Zhang, J. Khan, U. Farooq, H. Song, J. Tang, Efficient double buffer layer $Sb_2(Se_xS_{1-x})_3$ thin film solar cell via single source evaporation, Sol. RRL. (2018) 1800144, https://doi.org/10.1002/solr.201800144.
[9] B. Yang, S. Qin, D.-J. Xue, C. Chen, Y.-S. He, D. Niu, H. Huang, J. Tang, In sulfurization to generate $Sb_2(Se_xS_{1-x})_3$ alloyed films and their application for photovoltaics, Progr. Photovoltaics: Res. Applic. 25 (2017) 113–122, https://doi.org/10.1002/pip.2819.
[10] Y. Xie, K. Li, X. Li, F. Gao, X. Xiong, G. Zeng, B. Li, Fabrication of Sb_2S_3 solar cells by close space sublimation and enhancing the efficiency via co-selenization, Mater. Sci. Semicond. Process. 142 (2022) 106451, https://doi.org/10.1016/j.mssp.2022.106451.
[11] K. Li, Y. Xie, B. Zhou, X. Li, F. Gao, X. Xiong, B. Li, G. Zeng, M. Ghali, Fabrication of closed-space sublimation $Sb_2(Se_xS_{1-x})_3$ thin-film based on a single mixed powder source for photovoltaic application, Opt. Mater (2021), https://doi.org/10.1016/j.optmat.2021.111659.
[12] C. Chen, Y. Yin, W. Lian, L. Jiang, R. Tang, C. Jiang, C. Wu, D. Gao, X. Wang, F. Fang, C. Zhu, T. Chen, Pulsed laser deposition of antimony selenosulfide thin film for efficient solar cells, Appl. Phys. Lett. 10 (1063/1) (2020) 5139467.
[13] S. Lu, Y. Zhao, X. Wen, D.J. Xue, C. Chen, K. Li, R. Kondrotas, C. Wang, J. Tang, $Sb_2(Se_xS_{1-x})_3$ thin-film solar cells fabricated by single-source vapor transport deposition, Sol. RRL. 3 (2019) 1800280.
[14] Y. Pan, X. Hu, Y. Guo, X. Pan, F. Zhao, G. Weng, J. Tao, J.Jiang C.Zhao, S. Chen, P. Yang, J. Chu, Vapor Transport Deposition of Highly Efficient $Sb_2(Se,S)_3$ Solar Cells via Controllable Orientation Growth, Adv. Funct. Mater. 31 (2021) 2101476.
[15] K. Li, Y. Lu, X. Ke, S. Li, S. Lu, C. Wang, S. Wang, C. Chen, J. Tang, Over 7% Efficiency of $Sb_2(Se,S)_3$ solar cells via V-shaped bandgap engineering, Sol. RRL. 4 (2020) 92000220.
[16] Peng Tang, Zi-Heng Huang, You-Xian Chen, Hu Li, Li-Quan Yao, Hui Li, Li-Mei Lin, Jin-Rui Cai, Ya-Lu Zhan, Dong Wei, Shui-Yuan Chen, Da-Qin Chen, Gui-Lin Chen, Spatial bandgap tailoring via a novel injection chemical bath deposition enables highly effcient carbon-based Sb2(S,Se)3 thin film solar cells, Chem. Eng. J. 477 (2023) 146722.
[17] Li-Quan Yao, Li-Mei Lin, Zhi-Ping Huang, Yu Mao, Hu Li, Wen-Wei Lin, Shui-Yuan Chen, Zhi-Gao Huang, Jian-Min Li, Gui-Lin Chen, A liquid medium annealing strategy for highly [041]/[141]-oriented planar antimony sulfide solar cells with 7.23% efficiency, Nano Energy 106 (2023) 108064.
[18] T.M. Razykov, J. Bekmirzoev, A. Bosio, B.A. Ergashev, D. Isakov, R. Khurramov, K. M. Kouchkarov, M.A. Makhmudov, A. Romeo, N. Romeo, M.S. Tivanov, Sh. B. Utamuradova, D.S. Bayko, L.S. Lyashenko, O.V. Korolik, A.A. Mavlonov, Structural and optical properties of Sb_xSe_y thin films obtained by chemical molecular beam deposition method from Sb and Se precursors, Solar Energy 254 (2023) 67–72.
[19] T.M. Razykov, K.M. Kuchkarov, M.S. Tivanov, D.S. Bayko, L.S. Lyashenko, B. A. Ergashev, A. Mavlonov, A.N. Olimov, R. Khurramov, D.Z. Isakov, M. Pirimmatov, Characteristics of thin Sb_2Se_3 films obtained by the chemical molecular beam deposition method for thin-film solar cells, Thin. Solid. Films. 774 (2023) 139844.
[20] T.M. Razykov, A.Kh. Shukurov, K.M. Kuchkarov, B.A. Ergashev, R.R. Khurramov, J.G. Bekmirzoyev, A.A. Mavlonov, Morphological and structural characteristics of Sb_2Se_3thin films fabricated by chemical molecular beam deposition, Appl. Solar Energy 55 (2019) 376–379.
[21] T.M. Razykov, A. Bosio, B. Ergashev, K.M. Kouchkarov, A. Romeo, N. Romeo, R. Yuldoshov, M. Baiev, M. Makhmudov, J. Bekmirzoyev, R. Khurramov, E. Fazylov, Growth and characterization of $Zn_xSn_{1-x}Se$ films for use in thin film solar cells, Solar Energy 193 (141) (2019) 519–522.
[22] Menglin Huang, Zenghua Cai, Shiyou Chen, Quasi-one-dimensional $Sb_2(Se,S)_3$ alloys as bandgap-tunable and defect-tolerant photocatalytic semiconductors, J. Chem. Phys. 153 (2020) 014703.
[23] Z. Cai, C.M. Dai, S. Chen, Intrinsic defect limit to the electrical conductivity and a two-step p-type doping strategy for overcoming the efficiency bottleneck of Sb_2S_3 -based solar cells, Sol. RRL. 4 (2019) 1900503.
[24] Shuaicheng Lu, Yang Zhao, Xixing Wen, Ding-Jiang Xue, Chao Chen, Kanghua Li, Rokas Kondrotas, Chong Wang, Jiang Tang, $Sb_2(Se_{1x}S_x)_3$ thin-film solar cells fabricated by single-source vapor transport deposition, Sol. RRL. 3 (2019) 1800280.
[25] M.D. Khan, S.U. Awan, C. Zequine, C. Zhang, R.K. Gupta, N. Revaprasadu, Controlled synthesis of $Sb_2(Se_{1x}S_x)_3$ ($0 \le x \le 1$) solid solution and the effect of composition variation on electrocatalytic energy conversion and storage, ACS. Appl. Energy Mater. 3 (2) (2020) 1448–1460.
[26] Liu Y, K.T.E. Chua, T.C. Sum, C.K. Gan, First-principles study of the lattice dynamics of Sb_2S_3, Phys. Chem. Chem. Phys. 16 (1) (2014) 345–350.
[27] C.J. Diliegros-Godines, J.S. Cruz, N.R. Mathews, M. Pal, Effect of Ag doping on structural, optical and electrical properties of antimony sulfide thin films, J. Mater. Sci. 53 (16) (2018) 11562–11573.
[28] Sven Ruhle, Tabulated values of the Shockley–Queisser limit for single junction solar cells, Solar Energy 130 (2016) 139–147.